International Journal of Mass Spectrometry 316–318 (2012) 174–181

Contents lists available at SciVerse ScienceDirect

International Journal of Mass Spectrometry

journal homepage: www.elsevier.com/locate/ijms

IRMPD spectroscopy b_2 ions from protonated tripeptides with 4-aminomethyl benzoic acid residues

Michael J. Kullman[a], Samuel Molesworth[a], Giel Berden[b], Jos Oomens[b,c], Michael Van Stipdonk[a,*]

[a] Department of Chemistry, Wichita State University, Wichita, KS, USA
[b] FOM Institute for Plasma Physics, Nieuwegein, The Netherlands
[c] University of Amsterdam, Science Park 904, 1098X Amsterdam, The Netherlands

ARTICLE INFO

Article history:
Received 3 December 2011
Received in revised form 10 January 2012
Accepted 12 January 2012
Available online 9 February 2012

Keywords:
ESI
IRMPD spectroscopy
Peptide fragmentation
Ion structure

ABSTRACT

Collision-induced dissociation (CID) of the peptide alanine-4-aminomethylbenzoic acid-glycine, A(AMBz)G generates a prominent b_2 ion despite a previous report [E.R. Talaty, T.J. Cooper, S.M. Osburn, M.J. Van Stipdonk, Collision-induced dissociation of protonated tetrapeptides containing β-alanine, γ-aminobutyric acid, ε-aminocaproic acid or 4-aminomethylbenzoic acid residues, Rapid Commun. Mass Spectrom. 20 (2006) 3443–3455.] which showed that incorporation of the aromatic amino acid into a peptide sequence inhibits generation of b_n ions formed by cleavage to the immediate C-terminal side of the residue. Infrared multiple photon dissociation (IRMPD) spectroscopy and density functional theory (DFT) calculations suggest that the b_2 ion generated from A(AMBz)G has an acylium structure. The b_2 ion generated from (AMBz)AG, in which the aromatic residue is situated at the amino-terminus, is instead a conventional oxazolone.

© 2012 Elsevier B.V. All rights reserved.

1. Introduction

Within the domain of *proteomics*, tandem mass spectrometry (MS/MS) and collision-induced dissociation (CID) are two of the most important tools used for peptide and protein identification [1,2]. Sequencing, whether done by comparison to known peptide fragmentation patterns, or by searching sequence databases with bioinformatics tools that attempt to predict fragmentation, is dependent, in part, on product ion distributions generated by CID [3,4]. Therefore, a clear understanding of peptide fragmentation mechanisms, energetics and dynamics is necessary to maximize the effectiveness of MS/MS based identification.

Using low-energy collision induced dissociation (CID), fragmentation of protonated peptides traditionally involves charge (proton) mediated reactions, in which cleavage of amide bonds leads to generation of *b*, *y*, and *a* ions that reveal sequence [5,6]. Development of the *mobile proton* model [7,8] of peptide fragmentation, and related amide bond cleavage pathways [1–3,9–14], has been focused primarily on proton mobilization. The *pathways in competition* (PIC) fragmentation model [14] use the mobile proton model as a foundation for understanding, but takes into account the structures and reactivity of key reactive configurations and primary fragments as well as transition states and their energies.

There is a great deal of evidence that N-terminal b_n type fragment ions have structures that include, at least in part, C-terminal oxazolone rings [9,15] and retain much of the primary sequence of the precursor peptide ion, though more recent experiments [16–23] strongly suggest that a macro-cyclic *b* ion isomer, or intermediate, can arise through cyclization of the linear, oxazolone-terminated *b* ions. These macrocyclic species can then open at different amide bonds to regain a linear, oxazolone terminated structure and appear to be more prevalent for b_4 and larger ions [20].

In a prior study, we examined the potential influence of the presence and position of a single β-alanine (βA), γ-aminobutyric acid (γAbu), ε-aminocaproic acid (Cap) or 4-aminomethylbenzoic acid (AMBz) residue on the tendency to form b_n- and y_n-type product ions, using a group of protonated tetrapeptides with general sequence XAAG, AXAG and AAXG (where X refers to the position of amino acid substitution) [24]. Our working hypothesis was that the 'alternative' amino acids would influence product ion signal intensities by inhibiting or suppressing either the nucleophilic attack or key proton transfer steps by forcing the adoption of large cyclic intermediates or blocking cyclization altogether. For example, βA and γAbu would force cyclization and/or intramolecular nucleophilic attack to proceed through 6 and 7 member rings that are kinetically and entropically less favored than the 5-member ring involved in formation of an oxazolone. The AMBz residue prevents cyclization and attack because of the rigid aromatic ring. Indeed, it was discovered that specific *b* ions were greatly diminished when

* Corresponding author.
E-mail address: Mike.VanStipdonk@wichita.edu (M. Van Stipdonk).

1387-3806/$ – see front matter © 2012 Elsevier B.V. All rights reserved.
doi:10.1016/j.ijms.2012.01.008

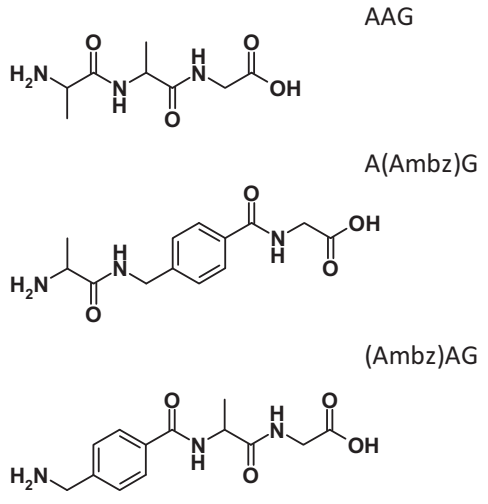

Fig. 1. Peptides used in the study of b_2 ion formation.

βA, γAbu residues are positioned such that they should interfere with the intramolecular nucleophilic attack step. The same b ions were eliminated when Cap and AMBz were placed in the same sequence positions.

Preliminary CID experiments performed by our group using tripeptides (Fig. 1) that included AMBz showed that alanine-AMBz-glycine, A(AMBz)G, generated an intense b_2 ion, despite the fact that formation of this species should have been inhibited by inclusion of the aromatic ring along the peptide backbone. A b_2 ion of similar intensity was observed for alanine-alanine-glycine, AAG, and AMBz-alanine-glycine (AMBz)AG; peptides for which the "oxazolone" pathway should generate the conventional *b*-type ion with the 5-member ring heterocycle at the C-terminus. In the present study, tandem mass spectrometry, infrared multiple photon dissociation (IRMPD) and density functional theory (DFT) calculations were used to investigate further the formation of b_2^+, and in particular to determine the structures of protonated A(AMBz)G and (AMBz)AG, and the b_2 ions generated from both peptides.

2. Experimental methods

2.1. Peptide synthesis and preparation

All model peptides were prepared using conventional solid-phase synthesis techniques [25] employing conventional coupling reagents, 9-fluorenylmethoxycarbonyl (Fmoc) amino acids and Fmoc-glycine loaded Wang resin and a custom-built, multiple reaction vessel peptide synthesis apparatus. All materials were purchased from (Thermo) Fisher Scientific (Pittsburgh, PA, USA) and used as received. Solutions of each peptide were prepared by dissolving the appropriate amount of solid material in a 1:1 (v:v) mixture of HPLC grade MeOH (Aldrich Chemical, St. Louis, MO, USA) and deionized H_2O to produce final concentrations of 10^{-5} to 10^{-4} M.

2.2. Ion trap mass spectrometry experiments

CID spectra were collected using a Finnigan LCQ-Deca ion-trap mass spectrometer (ThermoFinnigan, San Jose, CA, USA). Each of the peptide solutions were infused into the ESI-MS instrument using the incorporated syringe pump at a flow rate of 5 μl/min. The atmospheric pressure ionization stack settings for the LCQ (lens voltages, quadrupole and octapole voltage offsets, etc.) were optimized for maximum $(M+H)^+$ transmission to the ion trap mass analyzer by using the auto-tune routine within the LCQ Tune program. Helium was used as the bath/buffer gas to improve trapping efficiency and as the collision gas for CID experiments.

The $(M+H)^+$ ions were isolated for the initial CID stage (MS/MS) using an isolation width of 1.2–1.8 mass to charge (*m/z*) units. Product ions selected for subsequent CID (MS^3 experiments) were isolated using widths of 1.2–1.5 *m/z* units. For each stage, the width was chosen empirically to produce the best compromise between high precursor ion intensity and ability to isolate a single isotopic peak. The (mass) normalized collision energy (as defined by Thermo) was set between 20 and 25%, which corresponds the application of roughly 0.55–0.68 V tickle voltage to the end cap electrodes with the current instrument calibration. The activation *Q*, which defines the frequency of the applied R.F. potential, was set at 0.30. In all cases, the activation time employed was 30 ms. Spectra displayed represent the accumulation and averaging of at least 30 isolation, dissociation and ejection/detection steps.

2.3. ESI FT-ICR mass spectrometry

Previously established methods were used for generation of ions and the subsequent collection of IRMPD spectra [26–30]. Briefly, ESI was performed using a Micromass Z-Spray source. Ions were injected into a home-built Fourier transform ion cyclotron resonance (FT-ICR) mass spectrometer described in detail elsewhere [31]. Instrument operating parameters, such as desolvation temperature, cone voltage, and ion accumulation and transfer optics voltages, were optimized to maximize formation of $(M+H)^+$ ions, or b_2 ions generated by in-source CID, and transfer of the species to the ICR cell. Dry nitrogen (~80 °C) was used to assist in the desolvation process. Ions were accumulated for the duration of the previous FT-ICR cycle (approximately 5 s) in an external hexapole and injected into the ICR cell via a quadrupole deflector and an octapole RF ion guide.

2.4. Infrared multiple photon dissociation (IRMPD)

Infrared spectra were recorded by measuring the photodissociation yield as a function of photon wavelength. Precursor ions were irradiated using two FELIX macropulses (35 mJ per macropulse, 5 μs pulse duration, FWHM bandwidth ~0.5% of central λ). In the IRMPD process, a photon is absorbed when the laser frequency matches a vibrational mode of the gas-phase ion and its energy is subsequently distributed over all vibrational modes by intramolecular vibrational redistribution (IVR). The IVR process allows the energy of each photon to be dissipated before the ion absorbs another, which leads to promotion of ion internal energy toward the dissociation threshold via multiple photon absorption [32]. It is important to note that infrared spectra obtained using IRMPD are comparable to those collected using linear absorption techniques [33,34]. For the current experiments, the free electron laser wavelength was tuned between 6.25 and 11.2 μm in 0.04–0.1 μm increments. The intensity of product and un-dissociated precursor ions was measured using the excite/detect sequence of the FT-ICR-MS after each IRMPD step. The IRMPD yield was normalized to the total ion current, and linearly corrected for variations in laser power across the wavelength range scanned.

2.5. DFT geometry and frequency calculations

All DFT calculations were performed using the Gaussian 03 group of programs [35]. Full geometry optimizations for protonated A(AMBz)G, (AMBz)AG and various b_2 species were initiated using the hybrid B3LYP functional and the 3-21G* basis set on all atoms. Using the minima identified at this level of theory, relaxed scans were performed by rotating (through 360°) dihedral angles along the backbone in 3° steps to continue the search for

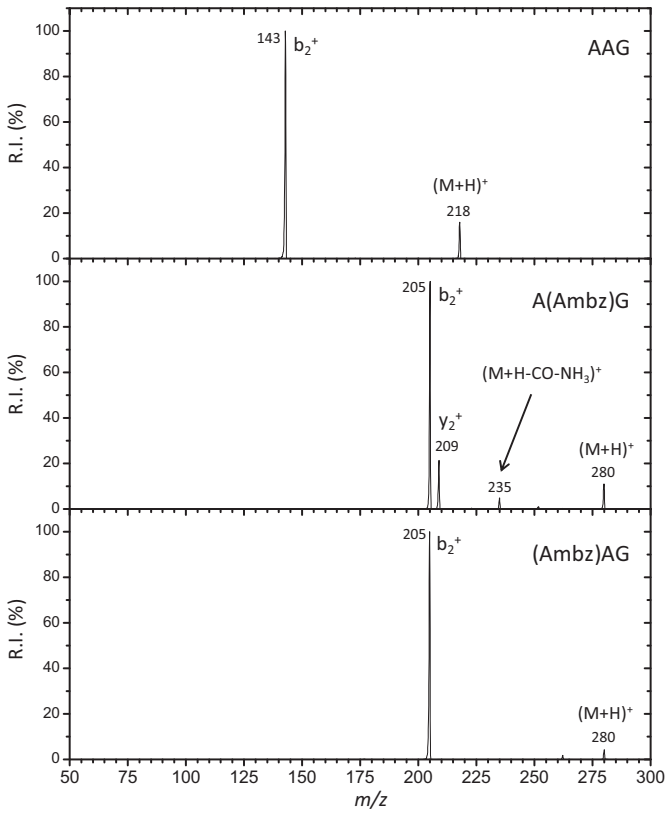

Fig. 2. CID spectra generated from protonated (a) AAG, (b) A(AMBz)G and (c) (AMBz)AG.

alternative structures. Mimina identified for all four ions were then re-optimized using the same functional and the 6-311+G(d,p) basis sets. Vibrational spectra and (zero-point corrected) relative energies were computed at the same level of theory. The vibrational frequencies are scaled by a factor of 0.98. This scaling factor was chosen empirically to produce a good correlation of peak positions in the experimental and theoretical IR spectra [36,37].

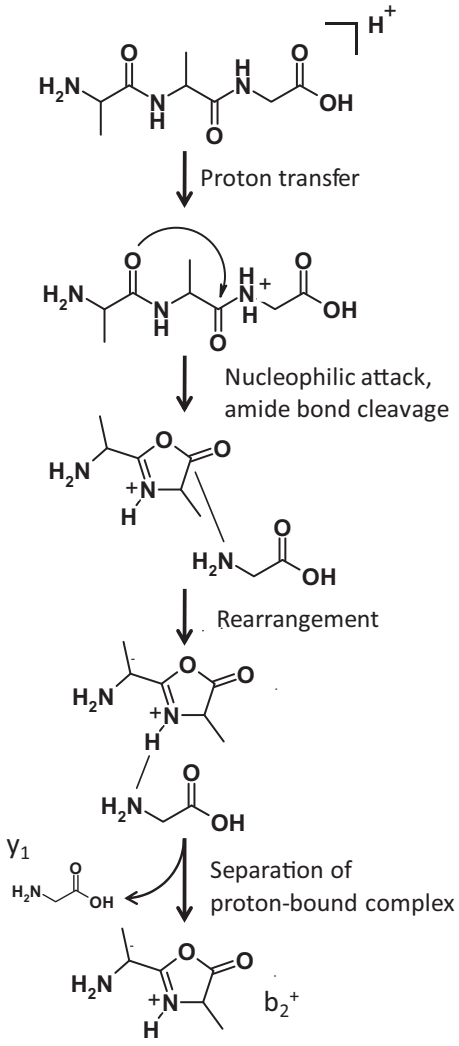

Scheme 1. General pathway showing formation of b_2^+ from protonated AAG via the oxazolone mechanism.

3. Results and discussion

3.1. CID of AAG, AAMBzG and AMBzAG

The CID spectra collected from protonated AAG, A(AMBz)G and (AMBz)AG are shown in Fig. 2. For each peptide, b_2^+ was the dominant product ion, appearing at *m*/*z* 143 for AAG and *m*/*z* 205 for both A(AMBz)G and (AMBz)AG. For A(AMBz)G (Fig. 2b), y_2^+ was observed at *m*/*z* 209, along with an ion at *m*/*z* 235 formed through the loss of CO and NH_3 (net 45 mass unit, u).

The y_2 ion is most likely generated along the so-called *a*/*y* pathway through elimination of imine and CO from the amino terminus of the peptide, in a charge-directed dissociation reaction initiated by migration of the added proton to the nitrogen of the N-terminal amide bond. DFT calculations of the reaction pathway suggest that direct cleavage of the amide bond produces a ternary complex that upon loss of weakly bound CO furnishes a proton-bound dimer composed of a protonated imine (N-terminal fragment) and truncated peptide (C-terminal fragment). The *y* ion is created by proton transfer from the imine to the C-terminal peptide fragment [14].

Generation of product ions that arise through elimination of CO and NH_3 from the C-terminus, a process that presumably leds to the species at *m*/*z* 235 in Fig. 2b, has been investigated in detail by Bythell et al. using protonated alanine-glycine-glycine (AGG) as a precursor [36]. Experiments revealed that the C-terminal amide bond is cleaved on the a_1–y_2 pathway and formation of a proton-bound dimer of GG and MeCH=NH was proposed. Among multiple possible reactions of the dimer, one involved rearrangement and elimination of NH_3 to form $[AGG+H-CO-NH_3]^+$. The putative reaction to create $[AGG+H-CO-NH_3]^+$ was evaluated further using ^{15}N labeling experiments and quantum chemical calculations, and a mechanism involving intermolecular nucleophilic attack and association of the GG and imine fragments, with subsequent loss of NH_3, was found to be more energetically favorable than expulsion of ammonia in an S_N2-type reaction.

The b_2 ions from protonated AAG and (AMBz)AG can be formed via the oxazolone pathway [14], as shown for the former in Scheme 1. There exists now a wealth of experimental (including IRMPD spectroscopy) and theoretical evidence for the generation of the oxazolone product from small peptides such as AGG, AAA and GGG [37–42]. The b_2 ion from A(AMBz)G presumably cannot be generated via the mechanism shown in Scheme 1 because the rigid aromatic ring prohibits the cyclization step and the intramolecular nucleophilic attack necessary to form the product ion. One would also assume that the rigid ring would inhibit the intramolecular proton transfer steps necessary for product ion formation. As noted earlier, AMBz markedly attenuates, if not completely eliminates, those b_n ions that cleavage to the immediate C-terminal side of the residue [24]. In the present study, elimination of 75 u from

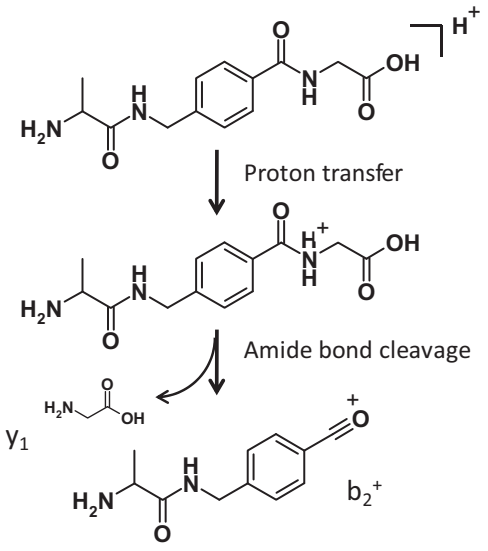

Scheme 2. Potential pathway for formation of b_2^+ as an acylium ion from A(AMBz)G.

A(AMBz)G to furnish b_2^+ probably instead involves direct cleavage of the C-terminal amide bond, as shown in Scheme 2, to leave an acylium ion.

In most cases, b_n ions fragment through the elimination of CO to generate a_n ions [14]. The CID spectra generated at the MS^3 stage (MS/MS/MS) for the b_2^+ ions derived from AAG, A(AMBz)G and (AMBz)AG are shown in Fig. S1 of the supporting information. For b_2^+ from protonated AAG (Fig. S1a) and (AMBz)AG (Fig. S1c), elimination of CO to make a_2^+ is the dominant pathway. However, the b_2 ion from A(AMBz)G fragments exclusively by elimination of NH_3. The mechanism by which NH_3 is eliminated is not known. Preliminary CID studies involving isotope labeled versions of the peptide show that the loss of NH_3 shifts to NH_2D when alanine with α-CD_3 is placed at the N-terminus. This suggests that NH_3 in general is eliminated by a pathway leaves an N-terminal vinyl group in the product ion. While the mechanism by which this ion is generated is perhaps worthy of independent study, the salient point is that b_2^+ derived from A(AMBz)G does not fragment in a fashion characteristic of oxazolones, consistent with the hypothesis that it adopts an alternative structure.

3.2. Structures predicted by DFT

The AAG peptide was included in the CID study as a control for comparison to the peptides that contain the AMBz residue. Because of time constraints during experiments with the FEL, an IR spectrum of protonated AAG was not collected, nor was a study of the lowest energy conformations of the peptide carried out. The lowest-energy structures for protonated A(AMBz)G and b_2^+ as an acylium species are shown in Fig. 3, with relative energies provided in units of kJ/mol. The lowest energy conformation of A(AMBz)G, structure **A(AMBz)G_p1**, is one with a protonated N-terminal amino group and an intramolecular hydrogen bonding interaction between the protonated amide and the N-terminal amide group. Structure **A(AMBz)G_p2** is a "charge solvated" conformation, 12.56 kJ/mol higher in energy than structure **A(AMBz)G_p1**, with the added proton residing on the O atom of the C-terminal amide group and an intramolecular hydrogen bonding interaction with the C-terminal acid group. A second intramolecular hydrogen bond is formed between the amino group and the H atom of the N-terminal amide. A charge solvated structure in which the hydrogen bonding interaction instead involves the —OH group of the C-terminus was several tens of kJ/mol higher than **A(AMBz)G_p2**, and was not pursued further.

In structure **A(AMBz)G_p3**, the N-atom of the C-terminal amide group is protonated, and an intramolecular hydrogen bond is formed with the O atom of the C-terminal acid group. While this structure is 69.39 kJ/mol higher in energy than **A(AMBz)G_p1**, it represents the amide N protonated structure that would cleave to furnish the acylium-type b_2 ion from protonated A(AMBz)G (Scheme 2). Elimination of 75 u in the dissociation reaction requires transfer of a proton to the C-terminal G residue. CID of A(AMBz)G ions generated from deuterated solvents showed a shift of the neutral loss to 78 u, consistent with the elimination of 3 exchangeable H atoms in the general fragmentation process (spectra not shown). Structure **A(AMBz)G_p3**, if populated during the dissociation reaction would allow the elimination of glycine from the C-terminus with 3 exchangeable protons (2 amide and 1 acid).

It is not possible to form an oxazolone species as b_2^+ from protoanted A(AMBz)G. The acylium ion structure, **A(AMBz)G_b2_A**, resembles the conformation of structure **A(AMBz)G_p3** for the precursor peptide, but with the acylium group on the aromatic ring. Alternative conformations for the b_2 ion, whether without the N-terminal hydrogen bonding interaction or with a cis-arrangement of the amide group, were significantly higher in energy and further optimization was not pursued.

The lowest-energy structures for protonated (AMBz)AG and the oxazolone b_2^+ product are shown in Fig. 4, with relative energies provided in units of kJ/mol. The lowest energy conformation for (AMBz)AG, structure (**AMBzA)G_p3**, is a charge solvated conformation in which the O atom of the N-terminal amide group is protonated, and a intramolecular hydrogen bonding interaction is formed with the O atom of the adjacent amide group. An alternative charge solvated structure, (**AMBz)AG_p2**, in which the O atom of the C-terminal amide group is protonated, is 35.14 kJ/mol in energy higher than (**AMBz)AG_p3**. The amine protonated conformation for (AMBz)AG, structure (**AMBz)AG_p2**, is 37.84 kJ/mol higher than (**AMBz)AG_p3**. While the structure includes two stabilizing hydrogen bonding interactions along the backbone, there are no functional groups capable of solvating the protonated amino group. This fact likely contributes to the higher relative energy of structure (**AMBz)AG_p1**.

The oxazolone structures shown for b_2^+ from (AMBz)AG differ primarily in the site of protonation. Structure (**AMBz)AG_b2_R** is lower in energy by ca. 27 kJ/mol, and is protonated at the N atom of the oxazolone ring. Structure (**AMBz)AG_b2_A** is instead protonated at the N-terminal amino group. The lower-energy (**AMBz)AG_b2_R** isomer is consistent with the proposed oxazolone pathway (Scheme 1), in which migration of the added proton to the C-terminal amide bond is followed by nucleophilic attack and ring-formation. The added proton is then eliminated as part of the complementary y_1 fragment and formation of a C=N bond within the ring furnishes the quaternary nitrogen to localize the charge on the b_2 ion.

Several attempts were made to locate minima for b_2^+ from (AMBz)AG that have acylium structures. Without imposing geometry constraints, the acylium species collapsed to structures (**AMBz)AG_b2_R** and (**AMBz)AG_b2_A** by attack of the amide carbonyl O atom on the C atom of the acylium group. Imposing constraints on the dihedral angles at the amide and acylium groups produced structures that had at least one imaginary frequency, identifying them as saddle points rather than true minima.

3.3. IRMPD spectroscopy of A(AMBz)G, (AMBz)AG and the b_2 ions

Fig. 5 compares the IRMPD spectra to those predicted for structures **A(AMBz)G_p1**, **A(AMBz)G_p2** and **A(AMBz)G_p3** of protonated A(AMBz)G (Fig. 5a–c, respectively) and for the acylium b_2

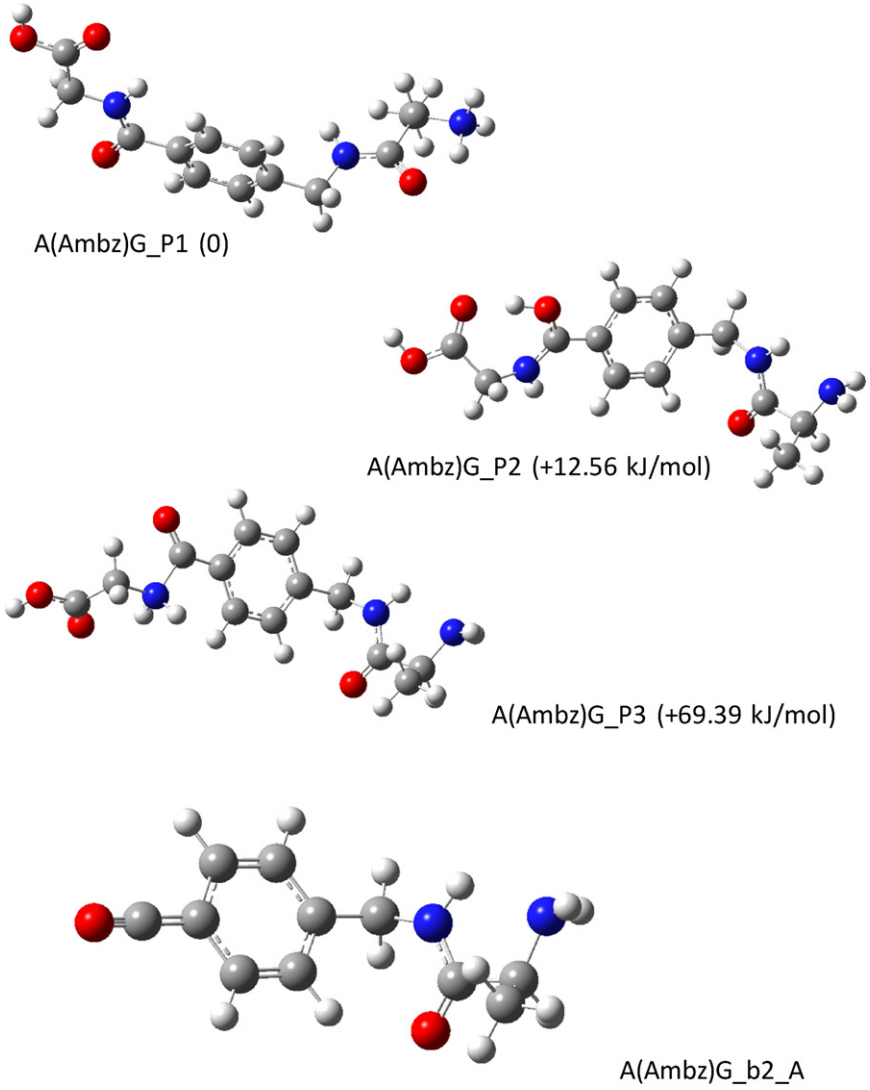

Fig. 3. Predicted structures (B3LYP/6-311+G(d,p) level of theory) for protonated A(AMBz)G and the potential acylium b_2 ion generated by CID.

ion (Fig. 5d). The IRMPD spectrum of protonated A(AMBz)G (solid line in Fig. 5a–c) contains absorptions at ca. 1270, 1390, 1515, 1705 and 1780 cm^{-1}. The best general agreement between the IRMPD spectrum and the spectra predicted by DFT is for structure **A(AMBz)G_p1**, consistent with the fact that the species is predicted to be lowest in energy among the respective structures.

Based on comparison to the theoretical spectrum for **A(AMBz)G_p1**, the absorptions at 1705 and 1780 cm^{-1} are assigned to the C=O stretches of the amide (amide I vibration) and acid groups, respectively. The collective amide II (C—N) vibrations, coupled to C—H wags of the aromatic ring, make up the absorption at 1515 cm^{-1} while the feature at 1390 cm^{-1} is assigned to backbone C—H stretches and wags. An absorption at 1270 cm^{-1} is not predicted for any of the lowest energy structures for **A(AMBz)G_p1**.

For the charge-solvated structure, **A(AMBz)G_p2**, DFT predicts that the C-terminal acid C=O stretch will be red-shifted to ~1725 cm^{-1} and is coupled to stretching of the C-terminal amide C=O group. The amide I vibration of the C-terminal amide group is predicted to appear as a minor peak at ca. 1539 cm^{-1} and to be coupled to C—C stretches of the aromatic ring. The amide II vibrations for the C-terminal and N-terminal amide groups are predicted to appear at ~1575 and 1517 cm^{-1}. For the structure featuring protonation of the C-terminal amide N atom (**A(AMBz)G_p3**), the C-terminal acid and N-terminal amide C=O stretches are reproduced well in the experimental IRMPD spectrum. However, the amide I vibration for the C-terminal amide group is predicted by DFT to be blue-shifted to 1850 cm^{-1}. Clearly, the predicted IR spectra for **A(AMBz)G_p2 and A(AMBz)G_p3** are in poorer agreement with the IRMPD spectrum, thus allowing assignment of the structure of protonated AAmbzG to **A(AMBz)G_p1**. This result is particular interesting given the assumption that structure **A(AMBz)G_p2** might be a necessary starting point for generation of b_2^+ by direct bond cleavage.

The IRMPD spectrum for the b_2 ion derived from A(AMBz)G (Fig. 5d) includes three prominent absorptions at ca. 1430, 1480, 1580 and 1700 cm^{-1}. These features are reproduced well by the spectrum predicted by DFT for structure **A(AMBz)G_b2_A**, strongly supporting the hypothesis that the species is an acylium ion. Using the theoretical spectrum vibrations for as a guide, the absorption at 1700 cm^{-1} is assigned to the C=O stretch of the amide bond. The absorptions at 1580 and 1430 cm^{-1} correspond to symmetric and asymmetric C—C stretch and C—H rock vibrations of the aromatic ring. The amide II stretch is assigned to the absorption at 1460 cm^{-1}. A diagnostic asymmetric C—C—O stretch of the acylium group is predicted by DFT to appear at 2237 cm^{-1}, which lies outside the region that was accessible with the FEL. Particularly important is the lack of a characteristic C=O stretch for oxazolone structures, which appears

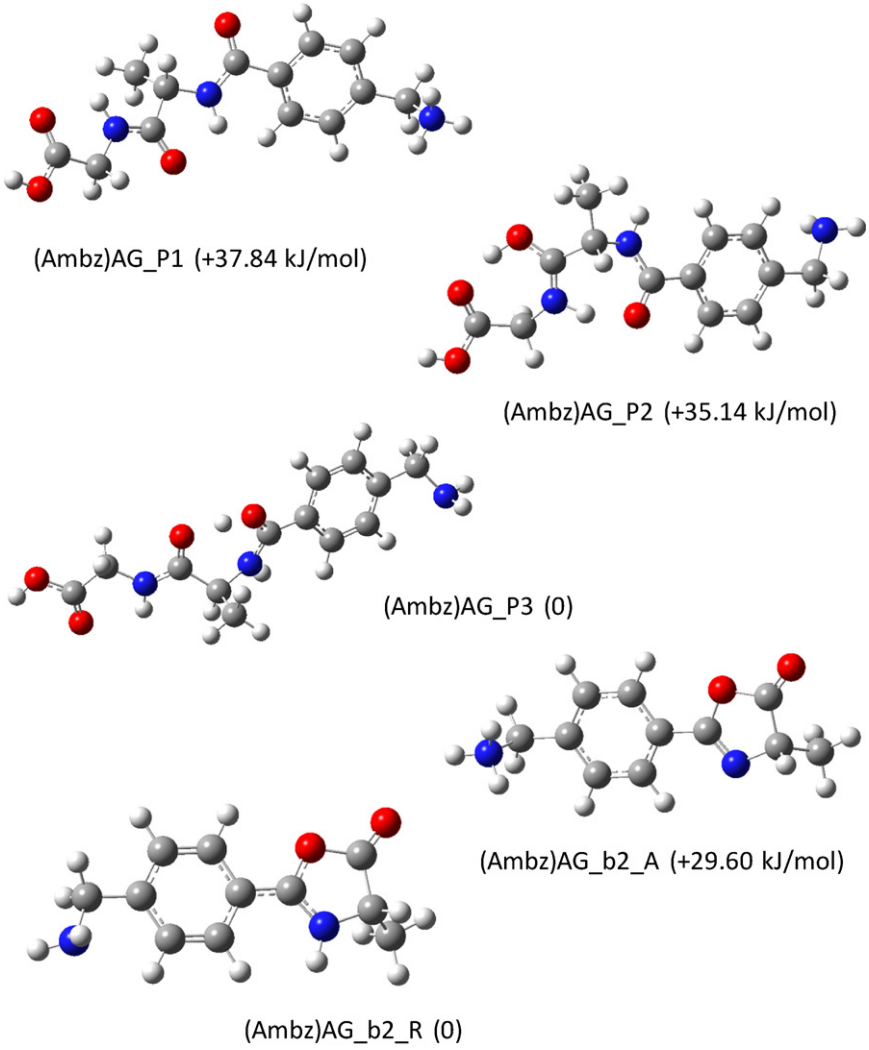

Fig. 4. Predicted structures (B3LYP/6-311+G(d,p) level of theory) for protonated (AMBz)AG and the oxazolone b_2 ion generated by CID.

in the region of 1900–1950 cm^{-1} [37,38,41,42], is the IRMPD spectrum of b_2^+ from protonated A(AMBz)G. This observation, and the excellent agreement between the theoretical and experimental spectra in the region scanned allows definitive assignment of the acylium type structure for b_2^+ derived from A(AMBz)G.

Fig. 6 compares the IRMPD spectra to those predicted by DFT for structures **(AMBz)AG_p1**, **(AMBz)AG_p2** and **(AMBz)AG_p3** of protonated (AMBz)AG (Fig. 6a–c, respectively) and for the two potential oxazolone structures for b_2^+ (Fig. 6d and e). For the protonated precursor ion, broad absorptions encompassing the range 1490–1660 cm^{-1} and a prominent feature at 1780 cm^{-1} are observed. The best general agreement between the IRMPD spectrum and the spectra predicted by DFT is for structure **(AMBz)AG_p3**, again consistent with the relative energies of the respective protonated isomers. Using the spectrum and vibrations predicted for **(AMBz)AG_p3** as a guide, the absorption at 1780 cm^{-1} is assigned to the acid carbonyl C=O stretch, while the envelope of absorptions from 1490 to 1660 cm^{-1} are assigned to the collective amide II vibrations. The amide I absorptions are predicted to appear at 1750 cm^{-1}, but are not resolved from the amide II vibrations.

For structure **(AMBz)AG_p1**, the amide I and amide II vibrations are predicted to appear at 1680 and 1490 cm^{-1}, respectively, positions that are in poor agreement with the IRMPD spectrum of protonated (AMBz)AG. The predicted position for the acid C=O stretch is reproduced well in the IRMPD spectrum. For structure **(AMBz)AG_p2**, agreement is reasonably good between DFT and IRMPD spectra in the region of the amide II vibrations (predicted to range from 1480 to 1620 cm^{-1}). However, the acid C=O stretch for structure **(AMBz)AG_p2** is predicted to be 40–50 cm^{-1} to the red of the observed position of 1780 cm^{-1}. Such a shift would be consistent with the adoption of a conformation in which the C-terminal acid group assisted with solvation of the added proton. Because of the relatively poor quality of the IRMPD spectrum, the possible presence of multiple structures for protonated (AMBz)AG cannot be ruled out entirely. However, our data suggests that the peptide most likely exists as a charge-solvated structure with protonation primarily at the O atom of the N-terminal amide group.

The IRMPD spectrum for the b_2 ion derived from (AMBz)AG was collected at two laser powers. Using the power employed to collect the spectra for protonated (AMBz)AG, the IR spectrum for the b_2 ion contained broad peaks and nearly 100% photodissociation yield. Attenuation using 8 dB produced narrower peaks in the IR spectrum and improved the comparison to those spectra predicted for the two minima predicted for b_2^+. The experimental IR spectrum for b_2^+ includes three prominent absorptions at ca. 1450, 1590 and 1930 cm^{-1}. The best agreement between experiment and theory is for **(AMBz)AG_b2_R** (Fig. 6e), in which protonation is on the oxazolone ring N atom. In particular, the positions of the oxazolone C=O and C–N stretches at 1930 and 1590 cm^{-1} is in good

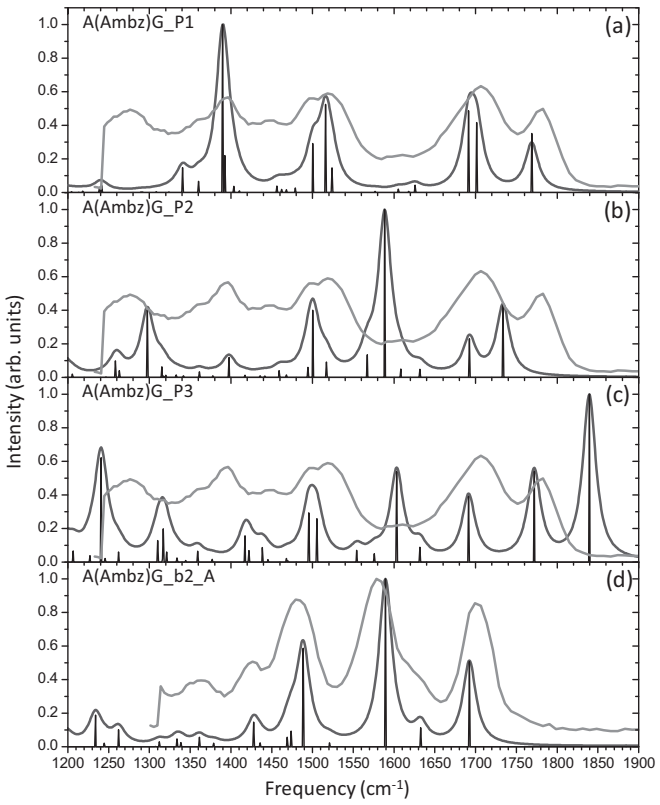

Fig. 5. Comparison of IRMPD and DFT spectra for protonated A(AMBz)G and the potential acylium b_2 ion generated by CID. Black trace: IRMPD spectrum of protonated A(AMBz)G; grey trace: predicted spectra.

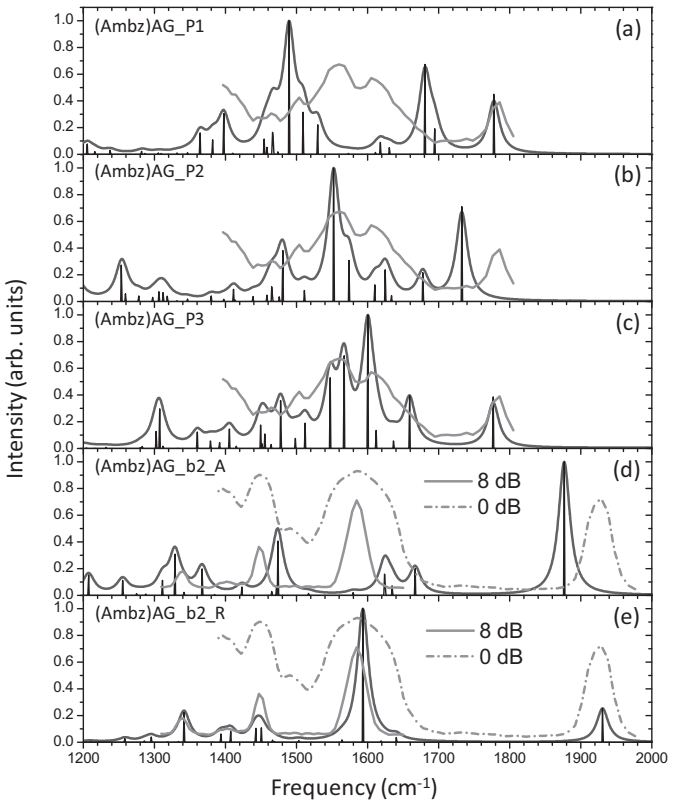

Fig. 6. Comparison of IRMPD and DFT spectra for protonated (AMBz)AG and the potential oxazolone b_2 ion generated by CID. Black trace: IRMPD spectrum of protonated A(AMBz)G; grey trace: predicted spectra.

agreement. The absorption at 1450 cm^{-1} is assigned to backbone C—H wags and stretches. For the amine protonated version of b_2, **(AMBz)AG_b2_A** (Fig. 6d), the oxazolone C=O stretch is predicted to shift to the red by 20 cm^{-1}, while the oxazolone ring C—N stretch shifts to the blue by 20 cm^{-1} relative to the position of the absorption in the IRMPD spectrum.

4. Conclusions

To summarize, collision-induced dissociation (CID) of the model peptide A(AMBz)G produced a prominent b_2^+ ion despite a previous report that showed generation of b_n ions is inhibited to the C-terminal side of the aromatic residue. IRMPD spectroscopy and density functional theory (DFT) calculations suggest that the b_2 ion generated from A(AMBz)G has an acylium structure, likely formed by direct cleavage of the C-terminal amide bond. IRMPD and DFT show that the b_2 ion generated from (AMBz)AG, in which the aromatic residue is situated at the amino-terminus, is instead a conventional oxazolone.

IRMPD clearly shows that gas-phase A(AMBz)G is protonated at the amino terminus. Formation of b_2^+ from a protonated tripeptide, whether through formation of an oxazolone, or as an acylium ion, requires transfer of proton to the C-terminal residue. The rigid aromatic ring of AMBz would appear to inhibit migration of the added proton from the amino terminus to the N atom of the C-terminal amide bond. Therefore, it is not clear how the acylium species is generated through a process that involves proton transfer, such as that shown in Scheme 2, particularly given the poor match between the IRMPD spectrum and the vibrations predicted for structure **A(AMBz)G_p3**. It is possible that b_2^+ formation proceeds through a process that involves cleavage of the C-terminal amide bond, creation of a proton-bound ion-molecule complex within which a proton transfer reaction occurs to furnish the acylium ion and neutral glycine product. The dynamics of such a process is currently being explored using DFT calculations and will be reported at a later date.

Acknowledgments

This work was supported by a grant to MVS from the National Science Foundation (CAREER-0239800). Funds to purchase the LCQDeca mass spectrometer were provided by Wichita State University and the State of Kansas NSF EPSCoR program. SM acknowledges Hospira, Inc. for financial support of his graduate research. JO and GB are supported by the Nederlandse Organisatie voor Wetenschappelijk Onderzoek (NWO). Construction and shipping of the FT-ICR-MS instrument was made possible through funding from the National High Field FT-ICR Facility (grant CHE-9909502) at the National High Magnetic Field Laboratory, Tallahassee, FL, USA. The excellent support by Dr. B. Redlich and others of the FELIX staff is gratefully acknowledged.

Appendix A. Supplementary data

Supplementary data associated with this article can be found, in the online version, at doi:10.1016/j.ijms.2012.01.008.

References

[1] D.F. Hunt, J.R. Yates III, J. Shabanonowitz, S. Winston, C.R. Hauer, Proc. Natl. Acad. Sci. 83 (1986) 6233–6237.
[2] K. Biemann, Biomed. Environ. Mass Spectrom. 16 (1988) 99–111.
[3] H. Steen, M. Mann, Nat. Rev. Mol. Cell Biol. 5 (2004) 699–711.
[4] A.E. Nesvizhskii, O. Vitek, R. Aebersold, Nat. Methods 4 (2007) 787–797.
[5] P. Roepstroff, J. Fohlmann, Biomed. Mass Spectrom. 11 (1984) 601.
[6] I.A. Papayannopoulos, Mass Spectrom. Rev. 14 (1995) 49.

[7] A.R. Dongre, J.L. Jones, A. Somogyi, V.H. Wysocki, J. Am. Chem. Soc. 118 (1996) 8365–8374.
[8] V.H. Wysocki, G. Tsaprailis, L.L. Smith, L.A. Breci, J. Mass Spectrom. 35 (2000) 1399–1406.
[9] T. Yalcin, I.G. Csizmadia, M.B. Peterson, A. Harrison, J. Am. Soc. Mass Spectrom. 7 (1996) 233–242.
[10] B. Paizs, G. Lendvay, K. Vekey, S. Suhai, Rapid Commun. Mass Spectrom. 13 (1999) 525–533.
[11] B. Paizs, S. Suhai, J. Am. Soc. Mass Spectrom. 15 (2004) 103–113.
[12] B. Paizs, S. Suhai, Rapid Commun. Mass Spectrom. 16 (2002) 375–389.
[13] M.J. Polce, D. Ren, C. Wesdemiotis, J. Mass Spectrom. 35 (2000) 1391–1398.
[14] B. Paizs, S. Suhai, Mass Spectrom. Rev. 24 (2004) 508–548.
[15] T. Yalcin, C. Khouw, I.G. Csizmadia, M.R. Peterson, A.G. Harrison, J. Am. Soc. Mass Spectrom. 6 (1995) 1165–1174.
[16] A.G. Harrison, A.B. Young, C. Bleiholder, S. Suhai, B. Paizs, J. Am. Chem. Soc. 128 (2006) 10364–10365.
[17] F. Riba-Garcia, K. Giles, R.H. Bateman, S.J. Gaskell, J. Am. Soc. Mass Spectrom. 19 (2008) 609–613.
[18] C. Bleiholder, S. Osburn, T.D. Williams, S. Suhai, M. Van Stipdonk, A.G. Harrison, B. Paizs, J. Am. Chem. Soc. 130 (2008) 17774–17789.
[19] C. Jia, W. Qi, Z. He, J. Am. Soc. Mass Spectrom. 18 (2007) 663–667.
[20] S. Molesworth, S. Osburn, M. Van Stipdonk, J. Am. Soc. Mass Spectrom. 20 (2009) 2174.
[21] A.G. Harrison, J. Am. Soc. Mass Spectrom. 19 (2008) 1776–1780.
[22] A.G. Harrison, J. Am. Soc. Mass Spectrom. 20 (2009) 2248–2253.
[23] A.E. Atik, T. Yalcin, J. Am. Soc. Mass Spectrom. 22 (2011) 38–48.
[24] E.R. Talaty, T.J. Cooper, S. Osburn, M.J. Van Stipdonk, Rapid Commun. Mass Spectrom. 20 (2006) 3443–3455.
[25] W.C. Chan, P.D. White (Eds.), Fmoc solid phase peptide synthesis – a practical approach, Oxford University Press Inc., New York, 2000.
[26] G.S. Groenewold, J. Oomens, W.A. de Jong, G.L. Gresham, M.E. McIlwain, M.J. Van Stipdonk, Phys. Chem. Chem. Phys. 10 (2008) 1192.
[27] G.S. Groenewold, A.K. Gianotto, K.C. Cossel, M.J. Van Stipdonk, D.T. Moore, N. Polfer, J. Oomens, W.A. de Jong, L. Visscher, J. Am. Chem. Soc. 107 (2006) 4802.
[28] G.S. Groenewold, A.K. Gianotto, K.C. Cossel, M.J. Van Stipdonk, J. Oomens, N. Polfer, D.T. Moore, W.A. de Jong, M.E. McIlwain, Phys. Chem. Chem. Phys. 9 (2006) 596.
[29] G.S. Groenewold, A.K. Gianotto, M.E. McIlwain, M.J. Van Stipdonk, M. Kullman, D.T. Moore, N. Polfer, J. Oomens, I. Infante, L. Visscher, B. Siboulet, W.A. de Jong, J. Phys. Chem. A 112 (2008) 508.
[30] G.S. Groenewold, M.J. Van Stipdonk, W.A. de Jong, J. Oomens, G.L. Gresham, M.E. McIlwain, D. Gao, B. Siboulet, L. Visscher, M. Kullman, N. Polfer, Phys. Chem. Chem. Phys. 9 (2008) 1278.
[31] J.J. Valle, J.R. Eyler, J. Oomens, D.T. Moore, L.G. van der Meer, G. von Helden, G. Meijer, C.L. Hendrickson, A.G. Marshall, G.T. Blakney, Rev. Sci. Instrum. 76 (2005) 023103.
[32] V.N. Bagratashvili, V.S. Letokov, A.A. Makarov, E.A. Ryabov, Multiple Photon Infrared Laser Photophysics and Photochemistry, Harwood, Chur, Switzerland, 1985.
[33] D.T. Moore, J. Oomens, J.R. Eyler, G. von Helden, G. Meijer, R.C. Dunbar, J. Am. Chem. Soc. 127 (2005) 7243.
[34] J. Oomens, A.G.G.M. Tielens, B.G. Sartakov, G. von Helden, G. Meijer, Astrophys. J. 591 (2003) 968.
[35] M.J. Frisch, G.W. Trucks, H.B. Schlegel, G.E. Scuseria, M.A. Robb, J.R. Cheeseman, J.A. Montgomery Jr., T. Vreven, K.N. Kudin, J.C. Burant, J.M. Millam, S.S. Iyengar, J. Tomasi, V. Barone, B. Mennucci, M. Cossi, G. Scalmani, N. Rega, G.A. Petersson, H. Nakatsuji, M. Hada, M. Ehara, K. Toyota, R. Fukuda, J. Hasegawa, M. Ishida, T. Nakajima, Y. Honda, O. Kitao, H. Nakai, M. Klene, X. Li, J.E. Knox, H.P. Hratchian, J.B. Cross, V. Bakken, C. Adamo, J. Jaramillo, R. Gomperts, R.E. Stratmann, O. Yazyev, A.J. Austin, R. Cammi, C. Pomelli, J.W. Ochterski, P.Y. Ayala, K. Morokuma, G.A. Voth, P. Salvador, J.J. Dannenberg, V.G. Zakrzewski, S. Dapprich, A.D. Daniels, M.C. Strain, O. Farkas, D.K. Malick, A.D. Rabuck, K. Raghavachari, J.B. Foresman, J.V. Ortiz, Q. Cui, A.G. Baboul, S. Clifford, J. Cioslowski, B.B. Stefanov, G. Liu, A. Liashenko, P. Piskorz, I. Komaromi, R.L. Martin, D.J. Fox, T. Keith, M.A. Al-Laham, C.Y. Peng, A. Nanayakkara, M. Challacombe, P.M.W. Gill, B. Johnson, W. Chen, M.W. Wong, C. Gonzalez, J.A. Pople, Gaussian 03, Revision D.01, Gaussian, Inc., Wallingford, CT, 2004.
[36] B.J. Bythell, D.F. Barofsky, F. Pingitore, M.J. Polce, P. Wang, C. Wesdemiotis, B. Paizs, J. Am. Soc. Mass Spectrom. 18 (2007) 1291–1303.
[37] J. Oomens, S. Young, S. Molesworth, M. van Stipdonk, J. Am. Soc. Mass Spectrom. 20 (2009) 334–339.
[38] B.J. Bythell, U. Erlekam, B. Paizs, P. Maitre, Chem. Phys. Chem. 10 (2009) 883–885.
[39] X.A. Chen, J.D. Steill, J. Oomens, N.C. Polfer, J. Am. Soc. Mass Spectrom. 21 (2010) 1313–1321.
[40] A.C. Gucinski, A. Somogyi, J. Chamot-Rooke, V.H. Wysocki, J. Am. Soc. Mass Spectrom. 21 (2010) 1329–1338.
[41] S.H. Yoon, J. Chamot-Rooke, B.R. Perkins, A.E. Hilderbrand, J.C. Poutsma, V.H. Wysocki, J. Am. Chem. Soc. 130 (2008) 17644–17645.
[42] X. Chen, L. Yu, J.D. Steill, J. Oomens, N.C. Polfer, J. Am. Chem. Soc. 131 (2009) 18272–18282.